Aggregate Interference in Random CSMA/CA Networks

June Hwang[1], Jinho Choi[2], Riku Jäntti[3], and Seong-Lyun Kim[2(✉)]

[1] Samsung Electronics, Mobile Communications Business, Suwon, Korea
june77.hwang@samsung.com
[2] Department of Electrical and Electronic Engineering, Yonsei University, 50 Yonsei-Ro, Seodaemun-Gu, Seoul, Korea
jhchoi@ramo.yonsei.ac.kr, slkim@yonsei.ac.kr
[3] Department of Communications and Networking, School of Electrical Engineering, Aalto University, 00076 Aalto, Finland
riku.jantti@aalto.fi

Abstract. In this paper, we investigate the cumulative distribution function (CDF) of the aggregate interference in CSMA/CA networks measured at an arbitrary time and position. We assume that nodes are deployed in an infinite two-dimensional plane by the Poisson point process (PPP). To find the effective active node density we analyze the distributed coordinate function (DCF) dynamics in a common sensing area and obtain the steady-state power distribution. The results of a massive simulation using Network Simulator-2 (NS-2) show a high correlation with the derived CDF.

Keywords: Aggregate interference · CSMA/CA · DCF · Poisson point proce · NS-2

1 Introduction

1.1 Motivations

Due to the inherent scarcity of frequency spectrum and increasing wireless traffic demands, frequency reuse has become an essential key technological issue associated with contemporary wireless communication systems. Frequency reuse intrinsically causes interference between wireless links using the same frequency. Accordingly, the state of the aggregate interference at an arbitrary position in the random node topology has become of great importance. Currently, unlicensed spectrum is considered to be a supplementary spectrum of Long Term Evolution (LTE) in the license-assisted access (LAA) system in the 3rd Generation Partnership Project (3GPP). For the system, the main incumbent networks are wireless local area networks (WLANs) which are based on IEEE 802.11.

This work was supported by the National Research Foundation of Korea (NRF) grant funded by the Korea government (MSIP) (NRF-2014R1A2A1A11053234).

D. Noguet et al. (Eds.): CROWNCOM 2016, LNICST 172, pp. 424–436, 2016.
DOI: 10.1007/978-3-319-40352-6_35

Because of the widespread deployment of WLAN systems, initiation of LTE operation in the unlicensed spectrum must be done carefully. In this context, it is necessary to understand the characteristics of the aggregate interference of IEEE 802.11 networks. Furthermore, the interference can be controlled using the relationships discovered among the protocol parameters. Such control is useful in optimizing the operation of densely deployed WLAN and to protect incumbent systems against LTE interference for cases in which the system shares spectrum [1].

In this paper, we are interested in the aggregate interference of random carrier sense multiple access/collision avoidance (CSMA/CA) networks that are based on the IEEE 802.11 distributed coordination function (DCF). We test and analyze the interference at the protocol level, which reflects the contention and signaling processes of DCF. Consequently, the goal is to obtain the statistical inference of the aggregate interference and to verify the results via simulations. Our analysis tool is the stochastic geometry [2].

Because of the complexity, most of the previous work has focused on ALOHA-like systems in which the aggregate interference can be analyzed by assuming that the transmitting nodes have independent locations and behaviors [3]. In a network of CSMA/CA nodes, every communication entity first senses the ongoing transmission in the channel and then determines when to start transmitting. Consequently, transmission by a node will impact on its neighbors' channel access. To reflect the effects, the authors adopt the Matérn approximation on active node density to derive the optimal carrier sense threshold in a CSMA/CA network in [4,5]. However, they directly adopt the approximation without verifying the validity of the approximation for a realistic network situation.

To utilize the characteristics of aggregate interference in practical cases, we would like to find the aggregate interference distribution in practical CSMA/CA networks, not an ideal CSMA network. Modeling a practical network requires a hybrid method that considers the both dependent and independent point processes together. To capture the collision and idle time effects caused by imperfect contention of the real-life CSMA/CA operation, we propose modeling the system using the Poisson Point Process (PPP) with the *effective active node density*.

1.2 Summary of Contributions and Organization of this Paper

Our idea is to use the PPP for calculating the aggregate interference of the CSMA/CA network, but with a new density λ', called *effective active node density* reflecting all the CSMA parameters. Section 3 is devoted to describing how we obtain λ', and its verification by massive NS-2 simulations is contained in Sect. 4. For the readers who are more interested in our results, please directly jump to Sect. 4. Our paper has the following notable results:

– **The effective node density reflecting CSMA/CA MAC layer operation is derived in Sect. 3.**

– **The aggregate interference using our derived effective node density is verified using the NS-2 and MATLAB simulations in Sect. 4. The distribution of the CSMA/CA aggregate interference is neither normal nor log-normal distribution.**

2 Point Process for Modeling Random CSMA/CA Networks

In this section, we focus on determining which type of point process is suitable for modeling CSMA/CA networks. In the point process, a mark can be assigned to each point independently, which is useful for modeling node-oriented properties. In particular, the case in which the number of nodes in a network is Poisson-distributed and their positions at a given time instant are independent of each other, is adequately explained by means of the PPP. The method to derive the aggregate power emitted from points at an arbitrary position under the independent marked PPP was previously studied as a *shot noise field*.

2.1 Inappropriateness of PPP and Dependent Point Process

The PPP approach as it currently exists may be insufficient to model the CSMA/CA. The reason is that it does not reflect the carrier sensing philosophy. In the carrier sensing operation, a sensing node always senses the shared medium and it delays its transmission once it senses that the medium is busy. The result is that active nodes are affected by each other, which means that the process is not independent.

Let us now consider the dependent point process as a possible alternative. Here, the dependent point process means that some initially deployed points are discarded or selected by the metric relative to the other points' marks or locations. There are two dependent point processes that are most closely related to the modeling of CSMA/CA networks [3]: the Matérn hardcore (MHC) process and the simple sequential inhibition (SSI) point process. In [6], the authors compared the aggregate power distributions of PPP, MHC, and SSI with simulations, and concluded that SSI is most appropriate for modeling CSMA networks. However, their result is not fully acceptable because they considered neither the details of practical MAC layer parameters nor the channel characteristics. A related paper [7] tries to solve the above issue by considering the backoff timer. However, there is still no consideration of the collision case, and the problem of underestimating the node intensity has not been fully solved.

2.2 Revisit of PPP with a New Density

In real situations, the concurrent transmission in an exclusion area occurs with some probability, not with deterministic patterns. This stochastic characteristic of real networks can be appropriately modeled using the independent point

process. Therefore, we believe that a possible way to model a CSMA/CA network is again to use the independent PPP, but with a new effective active node density (λ') reflecting MAC layer operations.

For our analysis, we consider an infinite plane where the transmitting nodes are deployed randomly at positions specified by a Poisson distribution with intensity λ. Each node transmits with constant power p. The radio channel attenuates with the pass-loss exponent $\alpha = 4$ and Rayleigh fading.

3 Effective Active Node Density

In this section, we obtain the effective active node density, which is defined as the average number of transmitting nodes per unit area. To derive the density, we first introduce the concept of a *mutual sensing area* (Sect. 3.1). Then we derive the probability of a number of active nodes (Sect. 3.2) and the power distribution of the channel in that area (Sect. 3.3). Lastly, we obtain the effective active node density (Sect. 3.4).

3.1 Effective Carrier Sensing Range and Mutual Sensing Area

Let us introduce a CS range R such that a sensing node can sense any ongoing transmission in this range. Then within a disk of radius $\frac{R}{2}$, every node senses each other. We set this disk as the mutual sensing area.

CS is based on the threshold γ, i.e., if the sensed power level at a sensing node is greater (or lower) than γ, a sensing node regards the channel as busy (or idle). The definition of R can be also interpreted as a minimum energy detection boundary. We assume that there is a dominant interferer near the sensing node because the energy detection is most affected by the strongest interferer at large CS threshold. Then, the CS probability versus the distance to this interferer is calculated as follows:

$$\mathbb{P}[\text{Channel is busy}] = \mathbb{P}[\frac{p_i}{r^4} + \nu \geq \gamma], \tag{1}$$

where p_i is a random variable (RV) representing the product of the fading effect and the constant transmission power from a typical node i, r is the distance between the sensing node and the interferer, and ν is the receiver noise power. Considering Rayleigh fading, p_i follows $\text{Exp}(1/p)$ with a constant transmission power p.

Consequently, with the CS range R, we convert the stochastic CS to a deterministic one. First, the average residual sensing area is calculated by integrating the parts of the circumference, of which the radius and the center are r and the sensing node, respectively. The CS probability of a point on this circumference is from (1):

$$\int_0^\infty 2\pi r \cdot \mathbb{P}[\frac{p_i}{r^4} + \nu \geq \gamma]\mathrm{d}r = \int_0^\infty 2\pi r e^{-\frac{1}{p}(\gamma-\nu)r^4}\mathrm{d}r = \frac{\pi^{3/2}}{2\sqrt{\frac{\gamma-\nu}{p}}} \tag{2}$$

Assuming that the deterministic CS region should have the same average residual sensing area (sensing resolution) as the stochastic CS, we get the CS distance R as follows:

$$R = \frac{1}{\sqrt{2}}\left(\frac{\pi p}{\gamma - \nu}\right)^{1/4} \tag{3}$$

By using this deterministic CS distance, which we will call the *effective carrier sensing range*, the interference is regarded as Boolean at a given distance rather than stochastic.

Let us consider an infinite plane in which the nodes are randomly deployed. Assume that there is an arbitrary disk having a radius $R/2$ in the plane (mutual sensing area), where every node in this area can sense other nodes' transmissions according to the definition of the CS range R. By using the PPP, the number of deployed nodes in the mutual sensing area follows a Poisson distribution with the parameter $\lambda\pi(\frac{R}{2})^2$ as follows (Fig. 1):

$$\mathbb{P}[N = n] = \frac{\{\lambda\pi(\frac{R}{2})^2\}^n}{n!} \exp\left(-\lambda\pi\left(\frac{R}{2}\right)^2\right) \tag{4}$$

Once we know $\mathbb{P}[N = n]$, we derive the probability of the number of active nodes, N_a, in the mutual sensing area $\mathbb{P}[N_a = a|N = n]$ and the power distribution at an arbitrary time instant in the mutual sensing area.

3.2 Number of Active Nodes, N_a in a Mutual Sensing Area

For the explanation of this section, let us define the following probability first:

Definition 1. p_{on} is the probability that there are ongoing transmissions in a given mutual sensing area at a certain time.

Consider a given mutual sensing area H. Let the *residual sensing area* be defined as the sensing node's CS area, excluding H. The active node is defined here as the sensing node that has no ongoing transmissions in its residual sensing area. The CS results for each sensing node in H are random. Therefore, N_a is an RV that varies within $[0, N]$.

For a sensing node in H to be active, the CS result sensed from its residual sensing area must be idle, and that sensed from H must also be idle. We can find the distribution of N_a in H as in (5) when the probability p_{on} of

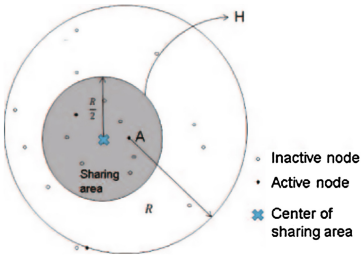

Fig. 1. If we pick up a certain mutual sensing area, every transmitting node in that area has its own residual sensing area. If there is no ongoing transmission in its residual sensing area, that node is the active node.

Definition 1 is given:

$$\mathbb{P}[N_a = a|N = n] = \sum_{\eta=0}^{8} P_{n,a,\eta} p_\eta, \quad a = 0, \ldots, n, \tag{5}$$

where

$$P_{n,a,\eta} = \binom{n}{a} \left(\frac{\eta}{8}\right)^a \left(1 - \frac{\eta}{8}\right)^{n-a}, \quad p_\eta = \sum_{D=0}^{8} O_\eta^D p_{on}^D (1 - p_{on})^{8-D}. \tag{6}$$

D and η are the discrete variables within $[0, 8]$. The value of O_η^D corresponding to D and η is given in Table 1. A description of the detailed derivation of (5), (6) and Table 1 is necessary but due to the space limitation, we only report the results.

Table 1. O_η^D

	D									
η	0	1	2	3	4	5	6	7	8	Sum(η)
0	0	0	0	8	38	48	28	8	1	131
1	0	0	0	24	24	8	0	0	0	56
2	0	0	12	16	8	0	0	0	0	36
3	0	0	8	8	0	0	0	0	0	16
4	0	0	8	0	0	0	0	0	0	8
5	0	8	0	0	0	0	0	0	0	8
6	0	0	0	0	0	0	0	0	0	0
7	0	0	0	0	0	0	0	0	0	0
8	1	0	0	0	0	0	0	0	0	1
Total	1	8	28	56	60	56	28	8	1	256

3.3 Steady-State Power Distribution in a Mutual Sensing Area

In this subsection, we derive the steady state power distribution in a mutual sensing area based on the distribution of number of active nodes in the area. We use the power distribution to obtain p_{on} in the next subsection. As shown in [8] and subsequent researches, the backoff stage of each node is random at a certain time, which can be elaborated through a two-dimensional Markov chain. We have two main quantities for addressing this: p_c is the collision probability for the transmission of each node, and τ is the transmission probability of a node at a randomly chosen time slot.

By following the notations of [5], we have the BEB dynamics with a maximum backoff stage m, a maximum retry limit K ($\geq m+2$), and an initial window size W_0. The probability τ that a node transmits in a randomly chosen time slot is:

$$\tau = \left\{ \frac{(1-p_c)W_0(1-(2p_c)^m)}{2(1-p_c^K)(1-2p_c)} + \frac{2^m W_0(p_c^m - p_c^K)}{2(1-p_c^K)} - \frac{1}{2} \right\}^{-1}. \tag{7}$$

Again, p_c is obtained as $p_c = 1-(1-\tau)^{N_a-1}$, where N_a is the number of active nodes. We can solve the system dynamics by solving independent Equations p_c and (7), and the existence of this solution is guaranteed by the fixed point theorem [8].

Then, the probability that i nodes transmit simultaneously at an arbitrary time slot, given that N_a transmitting nodes are deployed in a mutual sensing area, is computed as follows:

$$p_a(m) = \mathbb{P}[i = m | N_a = a] = \binom{a}{m} \tau^m (1-\tau)^{a-m}, \quad m = 0, \ldots, a. \tag{8}$$

Each transmitting node's operation in a mutual sensing area is synchronized, since the medium is sensed perfectly and every node uses the inner clock. Idle time is segmented into multiple slot times (σ). All events (idle, success and collision) can be distinguished by their own time lengths. At an arbitrary time slot called the *virtual time slot*, the medium in the mutual sensing area is in one of three events, and the virtual time slot has the random duration T_v. We assume that the payload size is PAY for all nodes. In the basic mode,

$$T_v = \begin{cases} \sigma, & \text{for idle,} \\ T_s^{BAS} (= PHY + \lceil \frac{(MAC+PAY)}{R_s} \rceil T_s + SIFS + ACK + DIFS), & \text{for success,} \\ T_c^{BAS} (= PHY + \lceil \frac{(MAC+PAY)}{R_s} \rceil T_s + DIFS), & \text{for collision,} \end{cases}$$

where PHY, $SIFS$, ACK, and $DIFS$ are the durations of the PHY header, SIFS (short interframe space) time, ACK packet, and DIFS (DCF interframe space) time, respectively. MAC, R_s and T_s are the MAC header size, symbol rate and symbol duration, respectively. Besides, superscript BAS denotes the basic mode and RTS denotes the RTS-CTS mode in this subsection.

T_v has the PMF induced from (8) such as $p_a(0)$, $p_a(1)$, and $1-p_a(0)-p_a(1)$, which are for idle, successful transmission, and collision, respectively. We derive the mean virtual time slot, $\mathbb{E}[T_v]$, using this PMF for each mode.

$$\mathbb{E}[T_v^{BAS}] = \sigma p_a(0) + T_s^{BAS} p_a(1) + T_c^{BAS}(1 - p_a(0) - p_a(1)),$$
$$\mathbb{E}[T_v^{RTS}] = \sigma p_a(0) + T_s^{RTS} p_a(1) + T_c^{RTS}(1 - p_a(0) - p_a(1)).$$

The distribution of the number of concurrent transmissions (which is also the power distribution) is based on this PMF. In each virtual time slot, the number of concurrent transmissions varies from 0 to N_a because it is possible that nobody transmits in a certain virtual time slot, even if there are some active nodes in the mutual sensing area. In the basic mode, nobody transmits during σ. During $SIFS$ and $DIFS$ in both the successful and collision slot times, nobody transmits. During the packet transmission time ($PHY + \lceil \frac{(MAC+PAY)}{R_s} \rceil T_s$ and ACK) in a successful slot, one node transmits, while multiple nodes transmit

during $PHY + \lceil \frac{(MAC+PAY)}{R_s} \rceil T_s$ in a collision slot. In the RTS-CTS mode, the power density is changed in the same manner. The actual power distribution, $\mathbb{P}[j\text{nodes transmit}|N_a = a]$ is obtained as follows:

$$B_a^{BAS}(j) = \frac{1}{\mathbb{E}[T_v^{BAS}]} \cdot \begin{cases} \sigma p_a(0) + (SIFS + DIFS) p_a(1) + DIFS(1 - p_a(0) - p_a(1)), & j = 0 \\ (PHY + \lceil \frac{(MAC+PAY)}{R_s} \rceil T_s + ACK) p_a(1), & j = 1 \\ (PHY + \lceil \frac{(MAC+PAY)}{R_s} \rceil T_s) p_a(j), & 2 \le j \le a. \end{cases} \quad (9)$$

With (9), the probability of a busy channel in a mutual sensing area p_{on} is $\sum_{j=1}^{a} B_a^{BAS/RTS}(j) = 1 - B_a^{BAS/RTS}(0)$.

3.4 Effective Active Node Density

So far, we have introduced a mutual sensing area using the spatial boundary of the Boolean CS operation, and have derived the distribution of the number of nodes, which is $\mathbb{P}[N = n]$ as in Eq. (4) in Sect. 3.1. We derived the probability of the number of active nodes for a given number of users in the mutual sensing area, $\mathbb{P}[N_a = a|N = n]$ as in Equation (5) in Sect. 3.2. Based on the transmission probability τ, the power distributions in the mutual sensing area can be calculated as in Eq. (9) in Sect. 3.3. With the results, we can formulate Eq. (10) from the definition of p_{on}. We can get the value of p_{on} by finding the intersection of the right and left hand sides of (10) numerically, which we will call p_{on}^*. In this section, $B_a(j)$ can be either of $B_a^{BAS}(j)$ and $B_a^{RTS}(j)$ according to the mode that we consider.

$$\begin{aligned} p_{on} &= \sum_{n,a} \sum_{j=1}^{a} B_a(j) = \sum_{n=0}^{\infty} \mathbb{P}[N = n] \sum_{a=0}^{n} \mathbb{P}[N_a = a|N = n] \sum_{j=1}^{a} B_a(j) \\ &= \sum_{n=1}^{\infty} \frac{\{\lambda\pi(\frac{R}{2})^2\}^n}{n!} e^{-\lambda\pi(\frac{R}{2})^2} \sum_{a=1}^{n} \sum_{\eta} P_{n,a,\eta} \{ \sum_{D} O_\eta^D p_{on}^D (1 - p_{on})^{8-D} \} \sum_{j=1}^{a} B_a(j) \quad (10) \end{aligned}$$

If we obtain p_{on}^*, the distribution of the number of transmitting nodes in the mutual sensing area can be derived as in (11), where the number of actual transmitting nodes (active and non-frozen) in the area is denoted by Z.

$$\mathbb{P}[Z = z] = \sum_{n=z}^{\infty} \left(\frac{\{\lambda\pi(\frac{R}{2})^2\}^n}{n!} e^{-\lambda\pi(\frac{R}{2})^2} \sum_{a=z}^{n} \mathbb{P}[N_a = a|N = n] \right) B_a(z), \text{ for } z \in \{0, 1, \dots\} \quad (11)$$

Then, the expected number of transmitting nodes is derived from this result:

$$\mathbb{E}[Z] = \sum_{z=0}^{\infty} z \cdot \mathbb{P}[Z = z] \quad (12)$$

The effective active node density is defined as the average number of transmitting nodes per unit area. Thus, we finally obtain the effective active node density as follows:

$$\lambda' = \frac{\mathbb{E}[Z]}{\pi(\frac{R}{2})^2}. \quad (13)$$

This is used in the cumulative distribution function (CDF) and the probability density function (PDF) of the aggregate interference. We plot the resulting CDF and PDF and compare these with the simulation results in Sect. 4.

4 Verification of the Analysis

In this section, we plot the effective node density (λ') of (13), and the CDF and PDF of the aggregate interference using λ'. Next, we compare the derived results with those obtained in the NS-2 and Matlab simulations. In the NS-2 simulation, the MAC/PHY parameters and channel model are given so that the CS radius R is determined to be 50, 70 and 100 (m).

4.1 Simulation Setup

MATLAB Simulation for MHC and SSI. We deployed the points using the MHC and SSI processes, as explained in [6], with MATLAB. The exclusion radius r_e is given as 70m. For a given number of nodes, the aggregated power was measured at O, which is the center of ball B with radius $R_M, R_S(= 282m)$ for MHC or SSI, respectively. The number of deployed nodes was generated using a Poisson distribution with the parameter $\lambda|B|$, where $\lambda(= 1, 2, 3, 4, 5 * 10^{-4})$ is the initial node density and $|B|$ is the area of ball B. We repeated this procedure for more than 100,000 iterations.

NS-2 Simulation for PPP. To verify the analysis results, we conducted simulations using NS-2 [9], which includes wireless PHY and MAC layer patches for the realistic IEEE 802.11 DCF standard [10]. This enabled us to realistically simulate the PHY and MAC stacks of the IEEE 802.11 DCF. The simulation parameters, which are the defaults for IEEE 802.11a PHY and MAC and are from the previous research.

The simulation conducted in this paper is full-scaled, which takes a long time to collect meaningful results for two reasons. First, each simulation per geometry scenario takes a long time. NS-2 traces all of the packet-level transactions with the received power recorded at every receiver. In the post-processing stage, the calculation of the received power from all of the ongoing transmissions at a measuring node takes computation time. Moreover, the simulation time itself (not the computation time) has to be long enough to reflect the steady-state behavior, which theoretically requires infinite investigation time. Second, to get a sound statistical inference of PPP, we repeat the per-geometry simulation 50 times since all of the resulting PDFs of the aggregate interference obtained from the simulations converge before 30 repetitions. We repeat this process for each combination of the PHY and MAC layer parameters.

Saturated traffic was assigned to all transmitters so that there was no idle time by the traffic itself during the simulations. The background grid for all of the simulation scenarios was always a 500 m by 500 m square. The transmission times for RTS, CTS, PPDU (PHY+MAC+PAY) with 500 B (or 1000 B) of payload and ACK were 52, 44, 728 (or 1396), and 44 (μs), respectively.

4.2 Discussions

Analysis results of p_{on} and λ'. p_{on} in this subsection refers to p^*_{on}, which can be found from (10), and is the final solution of p_{on} for simplicity of expression. In Fig. 2, the values of p_{on} are shown for various combinations of MAC parameters. The factor that affects p_{on} the most is the effective CS distance R, followed by λ, which is the initial node density. As λ increases, p_{on} naturally increases due to the increased congestion level. The p_{on} shows a mixture of linear and log functions. Within the same R, the combination that has the lowest p_{on} is the RTS mode and short payload. In general, RTS-CTS mode has a lower congestion level than the basic mode. With a large payload size, RTS-CTS mode is more favorable because two reasons: (1) a large payload in the basic mode makes for a higher congestion level, (2) the ratio of data transmission is large enough to compensate for RTS-CTS packet overheads.

This p_{on} was used in the new density λ' (13) and we plotted this as shown in the second figure of Fig. 2. This figure shows that the smaller R makes for a higher λ', which is the opposite of p_{on}. This is understandable, since a smaller R signifies more insensitivity to the interference. We expected the result of $R = 0$, the ALOHA system, to approach the line $\lambda' = \lambda$ in the figure. By showing the $\lambda' = \lambda$ line and the curves together, Fig. 2 also addresses the size of the gap between the original node density and effective node density, showing the effectiveness of CSMA/CA MAC. The bold curves are from the approximated node density modeled by the MHC. As shown in the figure, the variation of λ' is higher than that of MHC for varying λ. The figure shows the gap in the aggregate interference between simplified MHC and the real situation. As shown in the next section, our aggregate power distribution adopting λ' is the most accurate among the other point processes.

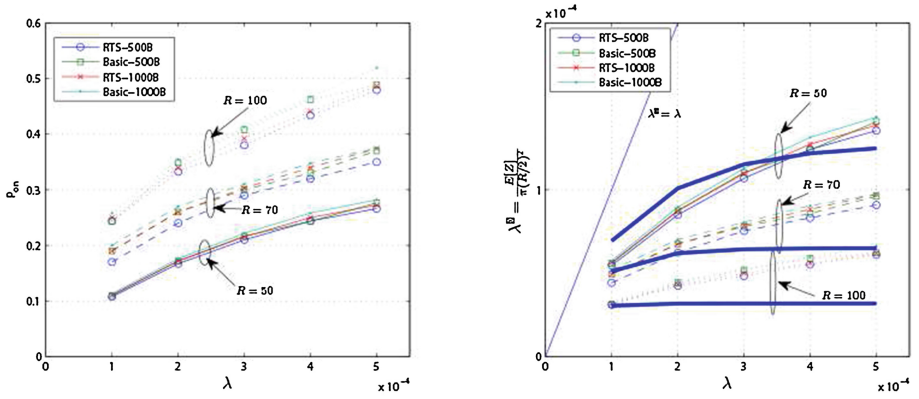

Fig. 2. P_{on} and new node density λ' versus λ for all combinations of MAC layer parameters. The thicker curves are from Matèrn hardcore process. (Color figure online)

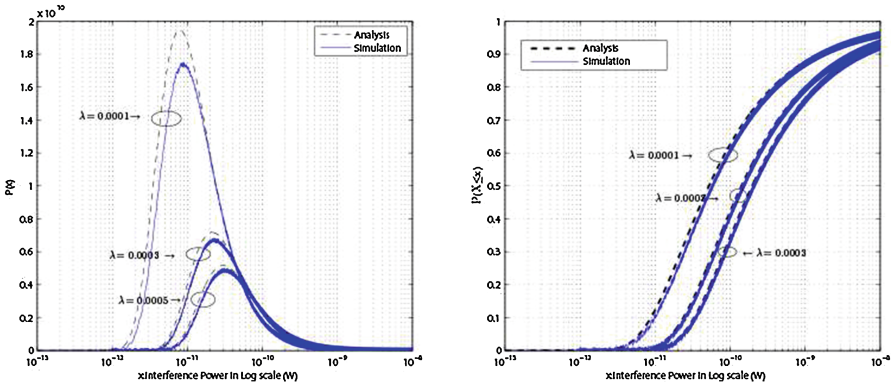

Fig. 3. Probability density and cumulative distribution of aggregate interference in the condition of RTS mode, 500B payload and $R = 70$(m).

Comparison of the Resulting Aggregate Interference with the Simulation. The PDF and CDF of the analysis in each node density showed high correlations with those of the NS-2 simulations as seen in Fig. 3.

Although at first glance they resemble a log-normal distribution, they are asymmetric based on the main lobe. They are definitely neither normal nor log-normal distributions. This is notable as some research efforts in the signal processing field assume that the aggregate interference follows normal (in dBm unit) or log-normal (in W unit) distributions. For the other features, the higher the mean of the aggregate power, the lower the probability of that mean value. Therefore, low-mean high-probability and high-mean low-probability patterns are shown in all of the results.

Compared with dependent point processes, at any given λ value, our analysis is the closest one to the simulation results, as depicted in Fig. 4. MHC and SSI do not have sufficient MAC and PHY layer parameters to reflect the real situation, while our analysis can model any combination of the system parameters, as in Fig. 5.

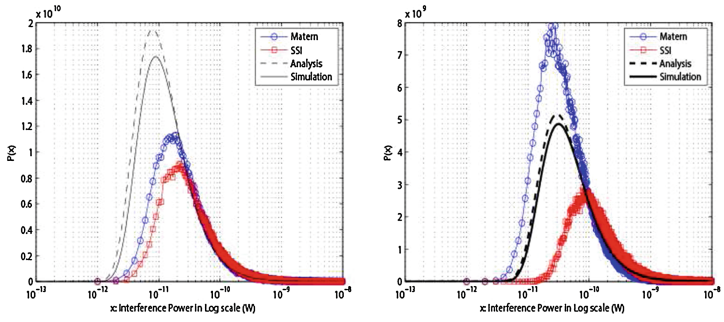

Fig. 4. Probability density of aggregate interference when λ is 0.0001 and 0.0005.

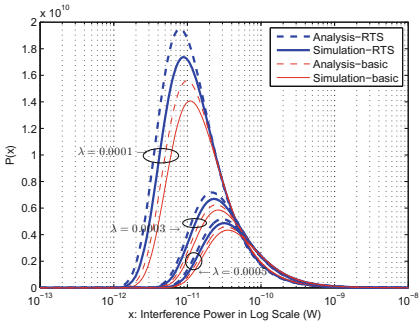

Fig. 5. Probability density of aggregate interference in the case of 500B payload and $R = 70$. (Color figure online)

As shown in the figures so far, our model of the aggregate interference has slightly lower values than that of the simulation in each case, because the simulator allows the *capture* situation. In our analysis, a collision between transmitters is regarded as a failure of transmission, and this increases each collided node's backoff stage. In contrast, there might be a successful transmission even when multiple nodes in a CS area are transmitting at the same time. This is because if the ratio of one incoming signal to the others is higher than a certain threshold, the stronger incoming signal can be decoded.

From these results, we learned the following lessons: If the network is required to maintain a lower interference than a certain level, there are multiple combinations of parameters that need to be controlled. Those controllable parameters are R, the transmission mode, payload size, etc. This can be used for the interference management in uncontrolled interference limited systems.

5 Conclusion

In this paper, we analyzed the aggregate interference from randomly deployed CSMA/CA nodes. Due to the imperfection of the CSMA/CA protocol, the transmission of each node in the network is not fully dependent, but is able to be modeled by independent point process with the new node density.

Our framework derived to find this value reveals the relation of the MAC parameters and the effective node density. Although the exact closed form expression of the interference distribution cannot be obtained, quite accurate interference distribution can be obtained by our methodology responding to the variation of MAC parameters. Furthermore, the sound simulation using NS-2 certifies that the analysis is enough to be used for optimizing the system parameters in uncontrolled WiFi hot spots or to protect incumbent systems in the case of secondary spectrum access.

References

1. Koufos, K., Ruttik, K., Jäntti, R.: 'Aggregate interference from WLAN in the TV white space by using terrain-based channel model. In: Proceedings of CROWNCOM (2012)
2. Baccelli, F., Błaszczyszyn, B.: Stochastic geometry and wireless networks volume 1: theory. Found. Trends Netw. **3**(3–4), 249–449 (2009)
3. Andrews, J., Ganti, R.K., Haenggi, M., Jindal, N., Weber, S.: A primer on spatial modeling and analysis in wireless networks. IEEE Comm. Mag. **48**(11), 156–163 (2010)
4. Kim, D.M., Kim, S.-L.: An iterative algorithm for optimal carrier sensing threshold in random CSMA/CA wireless networks. IEEE Comm. Lett. **17**(11), 2076–2079 (2013)
5. Hwang, J., Kim, S.-L.: Cross-layer optimization and network coding in CSMA/CA-based wireless multihop networks. IEEE/ACM Trans. Netw. **19**(4), 1028–1042 (2011)
6. Busson, A., Chelius, G., Gorce, J.-M.: Interference modeling in CSMA multi-hop wireless networks. Technical report INRIA, pp. 1–21, inria-00316029-ver3 (2009)
7. ElSawy, H., Hossain, E.: A modified hard core point process for analysis of random CSMA wireless networks in general fading environments. IEEE Trans. Commun. **61**(4), 1520–1534 (2013)
8. Bianchi, G.: Performance analysis of the IEEE 802.11 distributed coordination function. IEEE J. Sel. Areas Commun. **18**(3), 535–547 (2000)
9. Network Simulator-2. http://isi.edu/nsnam/ns/
10. Chen, Q., Schmidt-Eisenlohr, F., Jiang, D., Torrent-Moreno, M., Delgrossi, L., Hartenstein, H.: Overhaul of IEEE 802.11 modeling and simulation in NS-2. In: Proceedings of ACM MsWiM 2007 (2007)